Synchronization and partial synchronization experiments with networks of time-delay coupled Hindmarsh-Rose neurons

International Journal of Bifurcation and Chaos, Vol. 26, No. 7 (2016) 1650111 (20 pages)

DOI: 10.1142/S021812741650111X

Synchronization and Partial Synchronization Experiments with Networks of Time-Delay Coupled Hindmarsh–Rose Neurons

Erik Steur*
Faculty of Psychology and Educational Sciences,
Experimental Psychology Group,
Catholic University of Leuven, B-3000 Leuven, Belgium
erik.steur@ppw.kuleuven.be

Carlos Murguia†, Rob H. B. Fey‡ and Henk Nijmeijer§
Department of Mechanical Engineering,
Eindhoven University of Technology,
P. O. Box 513 5600 MB Eindhoven, The Netherlands
†*c.g.murguia@tue.nl*
‡*r.h.b.fey@tue.nl*
§*h.nijmeijer@tue.nl*

Received March 25, 2015; Revised November 9, 2015

We study experimentally synchronization and partial synchronization in networks of Hindmarsh–Rose model neurons that interact through linear time-delay couplings. Our experimental setup consists of electric circuit board realizations of the Hindmarsh–Rose model neuron and a coupling interface in which the interaction between the circuits is defined. With this experimental setup we test the predictive value of theoretical results about synchronization and partial synchronization in networks.

Keywords: Networks; synchronization; partial synchronization; time-delays; experiments.

1. Introduction

The emergence of synchronization in networks of coupled dynamical systems is a fascinating topic in various scientific disciplines ranging from biology, physics, and chemistry to social networks and technological applications. For instance, in biology, it is well known that thousands of fireflies light up simultaneously [Strogatz, 2003], and that groups of Japanese tree frogs (Hyla japonica) show synchronous behavior in their calls [Aihara *et al.*, 2011]. In medicine and neuroscience it is observed that clusters of synchronized pacemaker neurons regulate our heartbeats [Peskin, 1975], synchronized neurons in the olfactory bulb allow us to detect (and discriminate between) odors [Gray, 1994], and our circadian rhythms are synchronized to the 24-h day-night cycle [Czeisler *et al.*, 1980; Winfree, 2001]. Synchronization finds numerous applications in engineering sciences. An example is motion synchronization of mobile agents [Olfati-Saber & Murray, 2004; Ploeg *et al.*, 2014; Ren & Atkins, 2007; Sheikholeslam & Desoer, 1993; Stankovic *et al.*, 2000]. Particulary, [Ploeg *et al.*, 2014; Sheikholeslam & Desoer, 1993; Stankovic *et al.*, 2000] address the *platooning problem*, that is, the problem of designing intelligent vehicle/highway systems that can

*Current address: Department of Mechanical Engineering and Institute for Complex and Molecular Systems, Eindhoven University of Technology, P. O. Box 513 5600 MB Eindhoven, The Netherlands. E-mail: e.steur@tue.nl

significantly increase safety and highway capacity. The general objective of the platooning problem is to pack the driving vehicles together as tightly as possible in order to increase traffic flow while preventing amplification of disturbances throughout the string. This objective is achieved when the velocities of all the vehicles in the platoon are synchronized. Another example is synchronization in robotics, where multiple robots carry out tasks that cannot be achieved by a single one. For instance, in [Rodriguez & Nijmeijer, 2001], the authors propose a dynamic output controller that solves the synchronization problem of two (or more) robot manipulators in a master-slave coupling configuration. In [Sadowska *et al.*, 2011], the formation control problem for unicycle mobile robots interacting on symmetric graphs is studied. The range of engineering examples of network synchronization reaches way beyond coordinated motion. For instance, synchronization in power networks [Dorfler & Bullo, 2012], control of the directional sensitivity of smart antennas [Hutu *et al.*, 2009], and synchronization of microelectromechanical systems (MEMS), which has promising applications such as in neurocomputing [Hoppensteadt & Izhikevich, 2001] and improvements of signal-to-noise ratios [Agrawal *et al.*, 2011]. More examples of synchronous behavior in physics, biology, and engineering can be found in, for instance, [Blekhman, 1988; Pikovsky *et al.*, 2001; Strogatz, 2003; Winfree, 2001].

In this manuscript, we consider synchronization in network of systems that interconnect through linear time-delay couplings. These coupling functions are of the form

$$u_i(t) = \sigma \sum_j a_{ij}(y_j(t-\tau) - y_i(t)),$$

which we refer to as *transmission delay coupling*, and

$$u_i(t) = \sigma \sum_j a_{ij}(y_j(t-\tau) - y_i(t-\tau)),$$

which is called *full delay coupling*. The function $u_i(\cdot)$ denotes the input of system i, which has output $y_i(\cdot)$, $y_j(\cdot)$ is the output of a neighboring system j, $\tau \in \mathbb{R}_{>0}$ denotes the time-delay, the constants $a_{ij} \in \mathbb{R}_{\geq 0}$ are the interconnection weights, and $\sigma \in \mathbb{R}_{>0}$ is the coupling strength. In case of *transmission delay couplings*, the transmitted signals (the outputs of neighbors of system i) are delayed by τ units of time and compared with the current output of system i. These kind of couplings arise naturally in networked systems due to finite speed of propagation of signals such that system i can receive information about the state of its neighbors (via the outputs $y_j(\cdot)$) only after some time has lapsed. *Full delay couplings*, where all signals are time-delayed by an amount τ, may arise, for instance, when the systems are interconnected by a centralized control law. In that case, the central controller first has to sample the outputs of all the systems, then it has to compute the coupling inputs $u_i(\cdot)$ and, finally, the controller needs to communicate these inputs to the systems. Full delay coupling functions also appear in case that sensors and/or actuators have delays. A typical example is the sensor/actuator delay in car-following problems, where the amount of delay correlates with the human reaction time [Sipahi *et al.*, 2011].

Synchronization in networks of linearly coupled systems has been studied intensively. For instance, in [Wu & Chua, 1995; Pogromsky, 1998; Hale, 1997; Oguchi & Nijmeijer, 2011; Michiels & Nijmeijer, 2009; Murguia *et al.*, 2014] algebraic conditions are established to predict *synchronization* and *partial synchronization*. In [Grzybowski *et al.*, 2011], synchronization of two transmission delay coupled nonlinear systems is studied. Assuming fully actuated dynamics, the authors derive sufficient conditions for synchronization using Linear Matrix Inequalities (LMIs). In [Dahms *et al.*, 2012], the authors investigate the stability of synchronized states in delay coupled networks of fully actuated nonlinear systems. Using the master stability approach [Pecora & Carroll, 1998], they present a methodology for the characterization of stability of different patterns of synchronized dynamics (clusters) in networks with multiple time-delays, multiple coupling functions, and possible heterogeneous dynamics. Explicit relations between the structure of a network and conditions for synchronization are established in [Wu & Chua, 1996; Belykh *et al.*, 2004; Belykh *et al.*, 2005; Ünal & Michiels, 2013; Pogromsky, 2008]. Using extensive computer simulations, the authors in [Wang *et al.*, 2008, 2009, 2011a, 2011b] investigate front propagation and synchronization transitions in terms of the transmission time-delay and coupling strength in networks of diffusively coupled Rulkov and Hindmarsh–Rose neurons with additive noise. They found that for a fixed coupling strength, depending on the inherent oscillation frequency of individual

neurons, synchronization transitions appear as the time-delay is increased. Their simulation results show to be robust against variations in system size, intensity of additive noise, and the scaling exponent of the underlying scale-free network topology. They conclude that correctly tuned transmission delays are vital for assuring optimally synchronized neuronal networks and they should be regarded as important as the coupling strength.

Much less attention is devoted to the verification of theoretical synchronization results in real experimental setups. The focus of this paper is to test the validity of theory using an experimental setup that consists of electronic circuit board realizations of the (mathematical) Hindmarsh–Rose (HR) model neuron [Hindmarsh & Rose, 1984]. Particularly, this manuscript presents results of a series of experiments that are conducted to verify theoretical results about *full synchronization* [Steur & Nijmeijer, 2010], *partial synchronization* [Steur *et al.*, 2012], and *synchronization in relation to the network topology* [Steur *et al.*, 2014a]. We emphasize (partial) synchronization is understood in this manuscript as the asymptotic match of the states of (some of) the systems. The theoretical results presented in [Steur & Nijmeijer, 2010; Steur *et al.*, 2012; Steur *et al.*, 2014a] identify a large class of systems that can be synchronized by linear time-delay coupling, (of course, the HR model neuron belongs to this class). The conditions, which are of algebraic nature, are expressed at the level of the systems of the network. Whether or not the network synchronizes, or partially synchronizes, depends on the network structure and coupling parameters (time-delay τ and coupling strength σ). We remark that conditions for (partial) synchronization are global in the sense that it is not assumed the trajectories of the systems are initially close to synchrony.

In practical situations, however, the dynamics of the systems in the network cannot be expected to be perfectly identical. For instance, because the signals exchanged among the systems are contaminated with noise and/or there are small mismatches in the systems' parameters. Because of these inherent imperfections, we cannot expect that the systems perfectly (partially) synchronize. It is necessary to allow for a mismatch between them, which, of course, needs to be small enough in order to consider that the systems are "*practically synchronized*". To this end, we introduce the notions of *practical synchronization* and *practical partial synchronization*, which states that circuits may be called (partially) synchronized if, after some transient, the differences between their outputs are sufficiently small on a long finite time interval. The experiments with networks of coupled HR circuits shall indicate when our theoretical results, derived for identical systems and without any noise, (fail to) have sufficient predictive value in reality.

In Sec. 2, we describe the experimental setup. This setup consists of electrical circuit board realization of the HR model [Hindmarsh & Rose, 1984], which gives a description of the dynamics of the membrane potential of neurons. The coupling between these circuits is defined in a custom-made piece of hardware that is referred to as the *coupling interface*. In Sec. 3, we review our theoretical results described above. Section 4 introduces the notion *practical synchronization*, which states that systems can be considered synchronized in a practical sense if the differences between outputs of the systems are sufficiently small. Results on practical synchronization of two HR circuits with both transmission delay coupling and full delay coupling are presented. Our experimental findings on practical synchronization and practical partial synchronization in networks of HR circuits with transmission delay coupling or full delay coupling are given in Sec. 5. It is shown that, to a large extent, our theoretical results can explain and predict the synchronization phenomena observed in these experiments. Concluding remarks are provided in Sec. 6.

2. The Hindmarsh–Rose Neuron and the Experimental Setup

2.1. *A circuit realization of the Hindmarsh–Rose neuron model*

We consider networks of HR model neurons, whose dynamics are given by the following set of ordinary differential equations:

$$\begin{cases} \dot{z}_{i,1}(t) = 100(-y_i^2(t) - 2y_i(t) - z_{i,1}(t)), \\ \dot{z}_{i,2}(t) = 0.5(4y_i(t) + 4.472 - z_{i,2}(t)), \\ \dot{y}_i(t) = 100(-y_i^3(t) + 3y_i(t) - 8 + 5z_{i,1}(t) \\ \qquad\qquad - z_{i,2}(t) + E + u_i(t)). \end{cases} \tag{1}$$

Here $y_i(t) \in \mathbb{R}$ is the output of the ith model neuron, which represents its membrane potential, $z_i(t) := \mathrm{col}(z_{i,1}(t), z_{i,2}(t)) \in \mathbb{R}^2$ are the internal

states, $u_i(t) \in \mathbb{R}$ is an external input channel, which is used to communicate with other neurons, and $E \in \mathbb{R}$ is a constant parameter that defines the operating mode of the HR model neuron. In particular, for zero external input, $u_i(t) \equiv 0$, depending on the value of parameter E the membrane potential of the HR model neuron is either constant, spiking (i.e. a rapid rise and fall of the membrane potential), or continuous bursting, which refer to a mode of ongoing activity where spiking activity alternates with relatively long periods of quiescence. We set $E = 3.3$, for which the Hindmarsh–Rose neuron operates in a *chaotic bursting mode*. It is worth mentioning that we have obtained the system (1) by redefining the variables t, $z_{i,1}(t)$, $z_{i,2}(t)$, and $y_i(t)$ of the original model given in [Hindmarsh & Rose, 1984] according to

$$t \mapsto 100t,$$

$$z_{i,1}(t) \mapsto \frac{1}{5}(z_{i,1}(t) + 4),$$

$$z_{i,2}(t) \mapsto z_{i,2}(t) - 6,$$

$$y_i(t) \mapsto y_i(t) - 1.$$

The introduction of these new variables allows for an electronic circuit board realization of (1) with off-the-shelf components (resistors, capacitors, operational amplifiers and analog voltage multipliers) as the signals are now in the (linear) operating range of the electronic components. Figure 1(a) shows the electronic circuit board that implements Eqs. (1). A detailed description of the circuit diagram can be found in [Neefs *et al.*, 2010].

Each state, $z_{i,1}(t)$, $z_{i,2}(t)$, and $y_i(t)$ can be measured as a voltage on one of the five coaxial connectors shown in Fig. 1(a) at the right-side of the circuit board. The remaining two coaxial connectors are there to set the value of parameter E and provide the circuit its input signal $u_i(t)$. Figure 2(a) shows the states $z_1(t)$, $z_2(t)$, and $y(t)$ of (1) obtained by numerical integration of the equations in Matlab®, and Fig. 2(b) shows recorded states $z_1(t)$, $z_2(t)$, and $y(t)$ of an electrical circuit realization of Eqs. (1). There is a good qualitative match of measured signals and those obtained though numerical integration. Both the circuits and the mathematical model show irregular bursting behavior and the time-scales and amplitudes of the signals are nearly in the same range. Hereafter, we only show the outputs $y_i(t)$ of the Hindmarsh–Rose neurons.

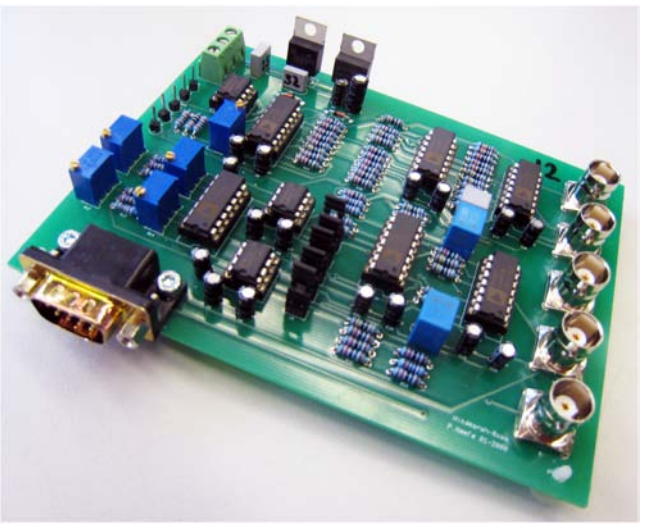

(a)

(b)

Fig. 1. The hardware of the experimental setup. (a) Electronic circuit realization of the Hindmarsh–Rose neuron and (b) coupling interface.

2.2. *The coupling interface and data acquisition*

The network topology and coupling functions, which are defined in Sec. 3, are specified in the *coupling interface* depicted in Fig. 1(b). This coupling interface allows us to construct networks with k HR neurons, $2 \leq k \leq 16$. The input and output channels of the HR circuit boards are connected via coaxial cables to the coupling interface in which the coupling inputs $u_1(t), \ldots, u_k(t)$ are computed as function of (delayed) outputs of the circuits $y_1(t-\tau), \ldots, y_k(t-\tau)$ and/or $y_1(t), \ldots, y_k(t)$. These coupling functions are defined in a custom-made software program (written in the C++ programming language), which is, after compiling, uploaded

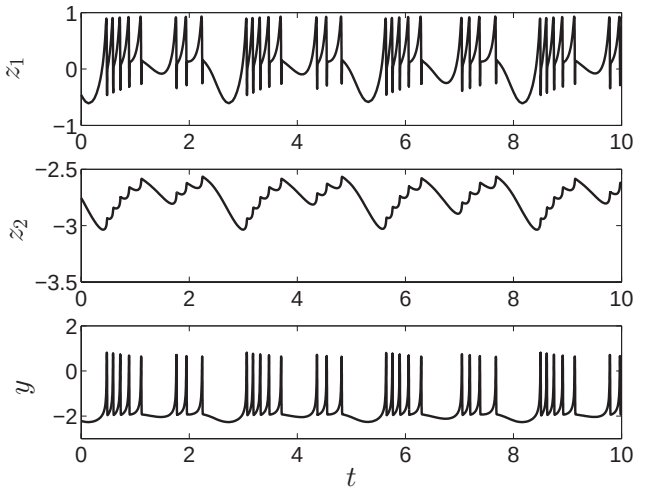

(a)

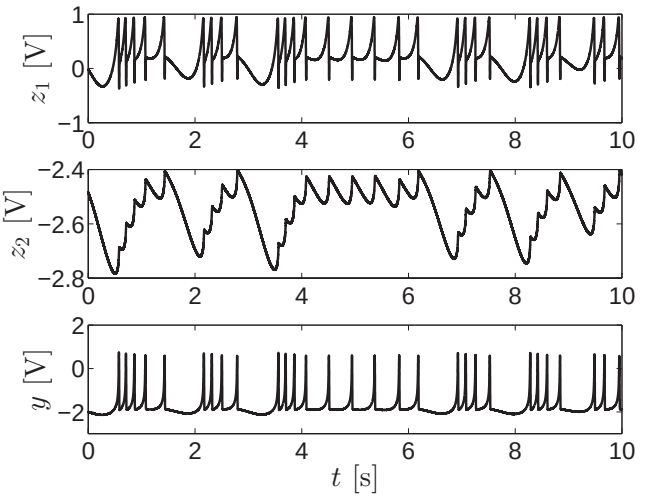

(b)

Fig. 2. Simulated solutions of (1) and recorded data of an electronic HR circuit without coupling. (a) Simulated solutions and (b) recorded data.

to the 210 [MHz] Atmel ARM© Thumb©-based AT91SAM9260 microcontroller at the heart of the coupling interface. In principle, any type of coupling can be implemented as the coupling functions are defined in software. The delays are emulated in software using circular buffers, whose lengths are proportional to the size of the delay. The coupling interface operates at a sampling rate of approximately 40 [kHz]. The outputs $y_i(t)$ of the circuits are sampled by a 16 bit ADC (with a range of -10 [V] to 10 [V]) and the inputs to the circuits $u_i(t)$ are generated using a 14 bit DAC (with a range of -10 [V] to 10 [V]). The sampling and updating of the signals happen simultaneously and the maximal throughput delay, which is equal for all connected circuits, is less than 80 [μs]. The data (time-traces) from the electronic HR circuits is obtained using a National Instruments PCIe-6363 multifunction data acquisition device with two BNC-2090A connector blocks. This data acquisition setup can measure up to 32 analog inputs (voltage range -10 [V] to 10 [V], 1 MS/s, 16 bit resolution) and has four analog output channels (voltage range -10 [V] to 10 [V], 2.86 MS/s, 16 bit resolution). We use only one analog output channel to specify E. The software that is used to acquire the data is National Instruments LabVIEW$^{\text{TM}}$ 2009 running on a HP wx4600 workstation with a 3.00 GHz Intel® Core$^{\text{TM}}$2 Duo CPU and 4 GB ram with Microsoft® Windows® XP Professional operating system. All data is plotted with Matlab® from The MathWorks, Inc.

3. Review of the Theoretical Results

In this section, we review the theoretical framework presented in [Steur & Nijmeijer, 2010; Steur *et al.*, 2012; Steur *et al.*, 2014a], which provides qualitative predictions about (partial) synchronization in networks with HR neurons. We represent the HR dynamics by the (more general) system

$$\begin{cases} \dot{x}_i(t) = f(x_i(t)) + Bu_i(t), \\ y_i(t) = Cx_i(t), \end{cases} \tag{2}$$

where $i \in \mathcal{V} := \{1, 2, \ldots, k\}$ and

$$x_i(t) = \begin{pmatrix} z_i(t) \\ y_i(t) \end{pmatrix}, \quad f(x_i(t)) = \begin{pmatrix} q(z_i(t), y_i(t)) \\ a(z_i(t), y_i(t)) \end{pmatrix},$$

$$B = C^\top = \begin{pmatrix} 0 \\ I_m \end{pmatrix}.$$

Here, $x_i(t) \in \mathbb{R}^n$ is the state of the system, $u_i(t) \in \mathbb{R}^m$ is the input, $y_i(t) \in \mathbb{R}^m$ is the output, and $f : \mathbb{R}^n \to \mathbb{R}^n$ denotes a sufficiently smooth function. Notice that the z_i-dynamics, which we shall refer to as the *internal dynamics*, do not depend explicitly on the input $u_i(t)$.

The network is represented by a graph $\mathcal{G} = (\mathcal{V}, \mathcal{E}, A)$ with

- $\mathcal{V}$ is the set of nodes;
- $\mathcal{E} \subset \mathcal{V} \times \mathcal{V}$ is the *ordered* set of edges;
- A is the weighted adjacency matrix.

We shall use the convention that an edge $(i, j) \in \mathcal{E}$ has its head at node $i \in \mathcal{V}$ and tail at node $j \in \mathcal{V}$.

The weighted adjacency matrix encodes the weights that the edges carry. That is, for a_{ij} being the ijth entry of the adjacency matrix A, a_{ij} is a positive real constant if and only if $(i,j) \in \mathcal{E}$, and $a_{ij} = 0$ otherwise. Given a node $i \in \mathcal{V}$, we define $\mathcal{N}_i := \{j \in \mathcal{V} \,|\, (i,j) \in \mathcal{E}\}$ as the set of its neighbors, i.e. the set of all nodes that have edges pointing to node i. It is assumed that the graph $\mathcal{G}$ is *simple*, that is, any two nodes of $\mathcal{G}$ are joined by at most one edge and $\mathcal{G}$ does not contain any edges of the form (i,i), i.e. $i \notin \mathcal{N}_i$ for all $i \in \mathcal{V}$. In addition, we always assume that the graph $\mathcal{G}$ is *strongly connected*, which means that for any two of distinct nodes $i, j \in \mathcal{V}$ there exists a path (i.e. a sequence of directed edges) in $\mathcal{G}$ from i to j and there exists a path from j to i. We define the diagonal matrix $D := \mathrm{diag}(d_1, d_2, \ldots, d_k)$ where the constants $d_i := \sum_{j \in \mathcal{N}_i} a_{ij}$ define the total weight of edges pointing to node i. The matrix D is known as the weighted degree matrix. Finally, define the matrix $L := D - A$, which is known as the weighted Laplacian matrix. Note that matrix L is singular by construction. It is well-known that the zero eigenvalue of L is simple if L is the weighted Laplacian matrix of a strongly connected graph, cf. [Bollobas, 1998].

Systems (2) on $\mathcal{G}$ interact via either one of the following time-delay coupling functions:

- *transmission delay coupling*

$$u_i(t) = \sigma \sum_{j \in \mathcal{N}_i} a_{ij}[y_j(t-\tau) - y_i(t)]; \qquad (3)$$

- *full delay couplings*

$$u_i(t) = \sigma \sum_{j \in \mathcal{N}_i} a_{ij}[y_j(t-\tau) - y_i(t-\tau)]. \qquad (4)$$

The positive constant σ denotes the *coupling strength* and the non-negative constant τ is the time-delay. The constants $a_{ij} \geq 0$ are the entries of the weighted adjacency matrix A of the graph $\mathcal{G}$. Since the coupling strength is encompassed in the constant σ, it is to be assumed without loss of generality that

$$\max_{i \in \mathcal{V}} \sum_{j \in \mathcal{N}_i} a_{ij} = 1.$$

Note that in case of the transmission delay coupling (3) only the *transmitted signals* contain delays and in the full delay coupling (4) *all signals* contain delay. It is important to point out that if all the systems in the network asymptotically synchronize, that is, the solutions of the systems asymptotically match

$$x_i(t) \to x_j(t) \quad \text{as } t \to \infty \quad \text{for all } i, j \in \mathcal{V},$$

then full delay coupling (4) vanishes but transmission delay coupling (3) does *not*. We therefore say that transmission delay coupling is *invasive* and full delay coupling is *noninvasive*. Because coupling (4) is noninvasive, and systems (2) are identical, it follows that the synchronized state is forward invariant under the dynamics of the coupled systems. For the synchronized state to be forward invariant for the dynamics of coupled systems (1), (3), we assume that

$$\sum_{j \in \mathcal{N}_i} a_{ij} = 1 \quad \text{for all } i \in \mathcal{V}.$$

See Proposition 1 in [Steur & Nijmeijer, 2010] for further details. From now on, it is supposed that the above assumption is always satisfied for systems interacting through the transmission delay coupling (3).

The theoretical results provided below are given for networks in its most general form, i.e. directed networks with possibly asymmetric adjacency matrices. However, our experiments are restricted to undirected networks with symmetric adjacency matrices. The reasons for this restriction are two-fold:

- We have better predictions for the emergence of (partial) synchronization in networks with symmetric interactions. Our goal here is to verify our best predictions experimentally;
- Although our goal is not to model a real neuronal network, the systems in our network are a model of the spiking activity of neurons. Then the coupling functions (3) and (4) can be considered as models of *electrical synapses* (also called *gap junctions*), which are symmetric, cf. [Koch, 1999].

3.1. *Synchronization in networks of time-delay coupled systems*

Let us start with the following result from [Steur & Nijmeijer, 2010].

Theorem 1. *Consider k system (2) coupled through time-delay coupling (3) [or (4)] on a simple strongly connected graph $\mathcal{G}$. Assume that*

- *the solutions of the coupled systems are (uniformly, uniformly ultimately) bounded;*

- *there exists an* $(n-m)\times(n-m)$*-dimensional matrix* $P = P^\top > 0$ *such that the symmetric matrix*

$$\left(P\frac{\partial q}{\partial z_i}(z_i, y_i)\right) + \left(P\frac{\partial q}{\partial z_i}(z_i, y_i)\right)^\top$$

has all its eigenvalues negative and separated away from zero for all $(z_i, y_i) \in \mathbb{R}^n$.

Then, there exist two positive constants $\overline{\sigma}$ *and* $\overline{\chi}$ *such that if*

$$\sigma \geq \overline{\sigma} \quad \textit{and} \quad \sigma\tau \leq \overline{\chi},$$

the network of coupled systems (2), (3) [*or* (2), (4)] *synchronize.*

It is shown in [Steur & Nijmeijer, 2010] that the first assumption (about boundedness of solutions of the coupled systems) is satisfied if the systems have a property called strict semi-passivity. Loosely speaking, this strict semi-passivity property states that the systems have only a limited amount of available free energy. We emphasize that a boundedness property is essential for the synchronization problem to be well-defined.

The second assumption in Theorem 1 implies that the z_i-dynamics of system (2) are exponentially convergent with respect to its "input" $y_i(\cdot)$, cf. [Pavlov *et al.*, 2004; Steur & Nijmeijer, 2010]. This exponential convergence of the z_i-dynamics tells us that the asymptotic solution of the z_i-dynamics does not depend on initial conditions $z_i(t_0)$. In particular, an exponentially convergent system has a unique globally asymptotically stable steady-state solution that depends on the input to that system, cf. [Pavlov *et al.*, 2004]. This implies that if all outputs $y_i(t)$ of the HR neurons (1) are synchronized, then all "internal states" $z_i(t)$ synchronize.

It can be shown that the HR model neuron (1) is strictly semi-passive and its z_i-dynamics satisfy the second assumption of the theorem, cf. [Steur *et al.*, 2009]. This implies any network of HR model neurons with coupling (3) or (4) synchronizes provided that the coupling strength is sufficiently large and the product of coupling strength and time-delay is sufficiently small. The values of the thresholds $\overline{\sigma}$ and $\overline{\chi}$ defined in Theorem 1 depend, besides on the systems' dynamics (2), on the network topology. In case of coupling (4) (because this type of coupling is noninvasive), one can show that if the graph $\mathcal{G}$ is undirected (i.e. $(i,j) \in \mathcal{E} \Leftrightarrow (j,i) \in \mathcal{E}$) and $A = A^\top$, then

- the value of $\overline{\sigma}$ is inversely proportional to the smallest nonzero eigenvalue of the Laplacian matrix $L := D - A$;
- the value of $\overline{\chi}$ is inversely proportional to the largest eigenvalue of L,

cf. the proof of the theorem on synchronization in [Steur & Nijmeijer, 2010]. This implies almost immediately the following scaling result.

Theorem 2 [Steur *et al.*, 2014a]. *Suppose that the assumptions of Theorem 1 are satisfied such that* $k = 2$ *coupled systems* (2), (4) *synchronize for any*

$$(\sigma,\tau) \in \mathcal{S}^* := \{(\sigma,\tau) \in \mathbb{R}_{>0} \times \mathbb{R}_{\geq 0} | \overline{\sigma} \leq \sigma \textit{ and } \sigma\tau \leq \overline{\chi}\}.$$

Consider a network of $k > 2$ *coupled systems* (2), (4) *with* $\mathcal{G}$ *being an undirected graph with symmetric adjacency matrix* A. *Let*

$$0 = \lambda_1 < \lambda_2 \leq \cdots \leq \lambda_k$$

be the eigenvalues of the Laplacian matrix L. *Then the network with* $k > 2$ *HR model coupled systems* (2), (4) *synchronizes if*

$$(\sigma,\tau) \in \mathcal{S}_2 \cap \mathcal{S}_k,$$

with $\mathcal{S}_j := \{(\frac{\lambda_j}{2}\sigma, \tau) \in \mathcal{S}^*\}$, $j = 2, k$, *being a scaled copy of* $\mathcal{S}^*$ *with scaling-factor* $2/\lambda_j$ *over the* σ*-axis.*

3.2. *Partial synchronization in networks of time-delay coupled systems*

If the "coupling strength is low" or the "time-delay is large" a network may be unable to synchronize. It can then happen that a network shows a form of incomplete synchronization that is characterized by the asymptotic match of the states of some, but not all, systems. This type of incomplete synchronization is what we refer to as *partial synchronization*. Let $\Pi \in \mathbb{R}^{k\times k}$ be a permutation matrix and suppose that there exist solutions of the coupled systems (2), (3) or (2), (4) that satisfy

$$x(t) = (\Pi \otimes I_n)x(t), \quad \forall\, t \geq t_0, \tag{5}$$

where I_n is the $n \times n$ identity matrix, $\otimes$ denotes the Kronecker (tensor) product, and

$$x(t) = \mathrm{col}(x_1(t), \ldots, x_k(t)).$$

A solution of the form (5) is a *partially synchronized solution corresponding to* Π if $1 < \dim\ker(I_k - \Pi) < k$. The latter inequality excludes the cases of

- no synchronization of any of the systems (for $\dim\ker(I_k - \Pi) = k$);
- synchronization of all systems (for $\dim\ker(I_k - \Pi) = 1$).

Indeed, note that $\dim\ker(I_k - \Pi) = k$ if and only if $\Pi = I_k$; hence, (5) is reduced to $x(t) = x(t)$. An example of a permutation matrix Π for which $\dim\ker(I_k - \Pi) = 1$ is

$$\Pi = \begin{pmatrix} 0 & 1 & 0 & \cdots & 0 \\ 0 & 0 & \ddots & \ddots & \vdots \\ \vdots & \vdots & \ddots & 1 & 0 \\ 0 & 0 & \cdots & 0 & 1 \\ 1 & 0 & \cdots & 0 & 0 \end{pmatrix}$$

such that (5) becomes

$$x_1(t) = x_2(t),$$
$$x_2(t) = x_3(t), \ldots, x_{k-1}(t) = x_k(t),$$
$$x_k(t) = x_1(t),$$

i.e. the fully synchronized solution.

For a given permutation matrix $\Pi \in \mathbb{R}^{k\times k}$, $1 < \dim\ker(I_k - \Pi) < k$, we define

$$\mathcal{P}(\Pi) := \{\phi \in \mathcal{C}([-\tau, 0], \mathbb{R}^{kn}) \,|\, \phi(\theta) = \mathrm{col}(\phi_1(\theta), \ldots, \phi_k(\theta)) \in \ker(I_{kn} - \Pi \otimes I_n), -\tau \le \theta \le 0\},$$

with I_{kn} being the kn-dimensional identity matrix, the set of partially synchronized solutions on the interval $[-\tau, 0]$. Noticing that $\mathcal{C}([-\tau, 0], \mathbb{R}^{kn})$, the space of continuous functions from $[-\tau, 0]$ into $\mathbb{R}^{kn}$, is the natural state-space of the coupled systems (2), (3) or (2), (4), it makes sense to call the set $\mathcal{P}(\Pi)$ a *partial synchronization manifold* for (2), (3) or (2), (4) if and only if it is a forward invariant set under the dynamics of the coupled systems. Conditions for existence of partial synchronization manifolds are provided in the following lemma from [Steur *et al.*, 2014b].

Lemma 1 [Steur *et al.*, 2014b]. *For a given graph $\mathcal{G}$ and given permutation matrix $\Pi \in \mathbb{R}^{k\times k}$, the manifold $\mathcal{P}(\Pi)$ is a partial synchronization manifold for the coupled systems (2), (3) if and only if either one of the following two equivalent conditions is satisfied*:

(i) $\ker(I_k - \Pi)$ *is a right invariant subspace of* A;
(ii) *there exists a matrix* $X_A \in \mathbb{R}^{k\times k}$ *that solves*

$$(I_k - \Pi)A = X_A(I_k - \Pi).$$

The manifold $\mathcal{P}(\Pi)$ is a partial synchronization manifold for the coupled systems (2), (4) if and only if either one of the following two equivalent conditions is satisfied:

(iii) $\ker(I_k - \Pi)$ *is a right invariant subspace of* L;
(iv) *there exists a matrix* $X_L \in \mathbb{R}^{k\times k}$ *that solves*

$$(I_k - \Pi)L = X_L(I_k - \Pi).$$

In case the matrices Π and A (Π and L) commute, i.e. $\Pi A = A\Pi$ ($\Pi L = L\Pi$), then $X_A = A$ ($X_L = L$) solves the matrix equation of condition (ii) (condition (iv)). In this case, the matrix Π can be thought of as a relabeling of the nodes, in such a way that the network before and after the relabeling is identical. Condition (i) (condition (iii)) can be used to construct a permutation matrix Π that defines a partial synchronization manifold from repeated patterns in the right eigenvectors of the matrix A (matrix L). For partial synchronization to occur, we require these manifolds to contain an asymptotically stable subset. In what follows, first for transmission delay coupling (3), we present sufficient conditions for the asymptotic stability of these partial synchronization manifolds.

Theorem 3 [Steur *et al.*, 2012]. *Consider k systems (2) coupled through the transmission delay coupling (3) and let the assumptions of Theorem 1 be satisfied. Let $\mathcal{P}(\Pi)$ be a partial synchronization manifold for the coupled systems and suppose that there is a constant $c^* > 0$ such that*

$$\vartheta^T(I_k - \Pi)^T\left(I_k - \frac{1}{2}(X_A^T + X_A)\right)(I_k - \Pi)\vartheta \ge c^*\vartheta^\top(I_k - \Pi)^\top(I_k - \Pi)\vartheta$$

for every $\vartheta \in \mathbb{R}^k$. Then, there exist positive constants σ^* and χ^* such that if $\sigma > \sigma^*$ and $\sigma\tau < \chi^*$, then the set $\mathcal{P}(\Pi)$ contains a globally asymptotically stable subset.

Likewise, for full delay coupling (4), we have the following result.

Theorem 4 [Steur *et al.*, 2012]. *Consider k systems (2) coupled through the full delay coupling (4)*

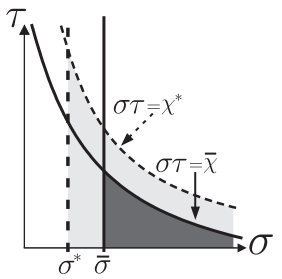

Fig. 3. The dark gray area represents the full synchronization region. The lighter gray area represents the partial synchronization region.

and let the assumptions of Theorem 1 be satisfied. Let $\mathcal{P}(\Pi)$ *be a partial synchronization manifold for the coupled systems and suppose that there is a constant* $c' > 0$ *such that*

$$\vartheta^T (I_k - \Pi)^T \left(\frac{1}{2}(X_L^T + X_L) \right) (I_k - \Pi)\vartheta \geq c' \vartheta^\top (I_k - \Pi)^\top (I_k - \Pi)\vartheta$$

for every $\vartheta \in \mathbb{R}^k$. *Then, there exist positive constants* σ' *and* χ' *such that if* $\sigma > \sigma'$ *and* $\sigma\tau < \chi'$, *then the set* $\mathcal{P}(\Pi)$ *contains a globally asymptotically stable subset.*

The problem of finding the constants c^* and c' satisfying (H3.1) and (H3.2) can be solved using singular value decomposition, see [Pogromsky, 2008]. Moreover, in the case of Theorem 4, if $X_L + X_L^T$ commutes with Π, then c' is the minimal eigenvalue of $\frac{1}{2}(X_L + X_L^T)$ under the restriction that the eigenvectors of $\frac{1}{2}(X_L + X_L^T)$ are taken from the set range$(I_k - \Pi)$.

We remark that multiple partial synchronization manifolds might coexist and also their conditions for being stable might coincide. To observe partial synchronization, it is obviously necessary that the values of the coupling strength and time-delay for which the partial manifold is stable do not coincide with those for which the full synchronization manifold is stable. Thus, it is necessary that

$$\begin{cases} \sigma^* < \overline{\sigma} \text{ and/or } \chi^* > \overline{\chi}, & \text{for coupling (3)}, \\ \sigma' < \overline{\sigma} \text{ and/or } \chi' > \overline{\chi}, & \text{for coupling (4)}, \end{cases} \quad (6)$$

with $\overline{\sigma}$ and $\overline{\chi}$ from Theorem 1. Necessary conditions for satisfying (6) are presented in the Appendix. An example where partial synchronization can be observed is schematically depicted in Fig. 3.

4. Practical Synchronization of Two Coupled HR Circuits

In this section, we report experimental results on synchronization of two coupled HR circuits. Recall that the HR model neuron (1) is strictly semi-passive and its z_i-dynamics satisfy the second assumption of Theorem 1. In particular, this last assumption implies that if the outputs of the HR neurons synchronize, then its internal z_i-dynamics has to synchronize as well. Note that our experimental setup allows us to measure the internal z_i-dynamics too. However, as we may conclude that the HR neurons synchronize if their outputs y_i synchronize, we will only show the output signals in this section and the next section.

In case that our HR circuits are perfectly identical, we may expect synchronization whenever the coupling strength exceeds some threshold value and, at the same time, the product of the time-delay and coupling strength is not too large. However, because of the inherent imperfections of the experimental setup, we cannot expect the neurons to be identical such that the differences between the outputs (and states) of circuits converge asymptotically to zero. It is necessary to allow for a mismatch between them, which, of course, needs to be small enough in order to consider the neurons to be "*practically synchronized*".

Definition 4.1 [Practical Synchronization]. Consider k dynamical systems with outputs $y_i(t) \in \mathbb{R}^m$, $i \in \mathcal{V} = \{1, 2, \ldots, k\}$, defined on an interval $[t_0, t_2)$. The k systems are said to be *practically synchronized with bound* ϵ, if there is a $t_1(\epsilon)$, $t_0 \leq t_1(\epsilon) < t_2$, such that $|y_i(t) - y_j(t)| < \epsilon$ for all $i, j \in \mathcal{V}$ and $t \in [t_1, t_2)$.

For notational convenience, we fix the value of ϵ and refer to *practical synchronization with bound* ϵ simply as *practical synchronization*. In all the following experiments, we say that the circuits practically synchronize if the eventual difference between the outputs does not exceed $\epsilon = 0.25$ [V]. Although this value of ϵ looks rather large, one has to realize that a small mismatch in the shapes or timing of the spikes results in a relatively large synchronization error. Figure 4(a) shows practical synchronization of two circuits using the full delay coupling with $\sigma = 0.55$ [−] and $\tau = 80$ [μs] (the throughput delay). The outputs of the two systems are almost indistinguishable with $\epsilon = 0.25$ [V]. Figure 4(b) shows that the synchronization error $y_1(t) - y_2(t)$ is within the

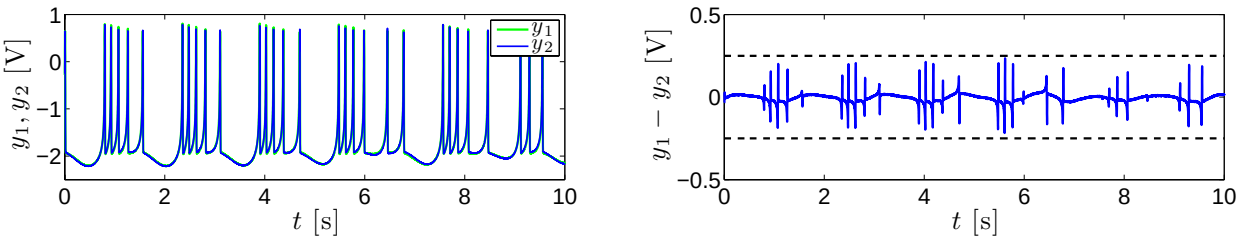

(a) (b)

Fig. 4. Practical synchronization of two full delay coupled electronic HR circuits for $\sigma = 0.55\,[-]$ and $\tau = 80\,[\mu s]$. (a) Recorded time-traces of the outputs of the two circuits and (b) time-trace of the difference in output signals. The horizontal dashed lines correspond to the bounds $\pm\epsilon = \pm 0.25\,[V]$.

bound $\epsilon = 0.25\,[V]$ and the errors are the largest when the practically synchronized circuits produce their spikes.

Figure 5 depicts the practical synchronization diagrams of the two coupled systems for transmission delay coupling [Fig. 5(a)] and full delay coupling [Fig. 5(b)], where we define the practical synchronization diagram to be the set of all (σ, τ) for which the coupled circuits practically synchronize with bound $\epsilon = 0.25\,[V]$. These practical synchronization diagrams are constructed by, for a fixed value of the time-delay τ, increasing the coupling strength from $0\,[-]$ to $10\,[-]$ and recording the values of σ for which the two coupled systems begin to practically synchronize and for which practical synchronization is lost. These points are indicated by the stars in Fig. 5. The practical synchronization diagrams, the shaded area in Fig. 5, are obtained through simple linear interpolation of the measured boundary points (the stars). Results for $\sigma > 10\,[-]$ cannot be presented because of hardware limitations; for values of the coupling strength $\sigma > 10$, we have observed that the coupling signals $u_1(t), u_2(t)$ become saturated.

The shape of the experimentally determined synchronization diagrams is a reasonable but not perfect match with the theoretical predictions presented in Theorem 1. However, we see that the two circuits practically synchronize if the coupling exceeds a certain threshold value. Moreover, for a fixed delay τ, an increase of coupling strength results in loss of practical synchronization but practical synchronization is regained by lowering the value of the delay. There are many reasons why the match between experiments and theory is not perfect. First of all, our theoretical results are sufficient results, which may be too conservative. On the other hand, in the experimental setting, the systems are not perfectly identical, signals are corrupted with noise and some additional errors are

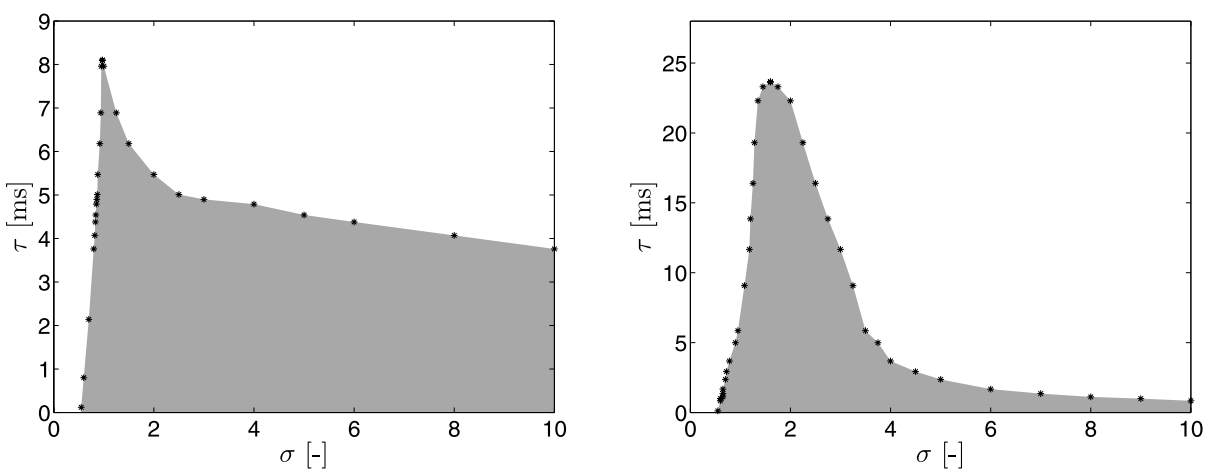

(a) (b)

Fig. 5. Approximated practical synchronization diagrams (shaded area) for two coupled HR circuits. The stars indicate the measured boundary points. (a) Transmission delay coupling and (b) full delay coupling.

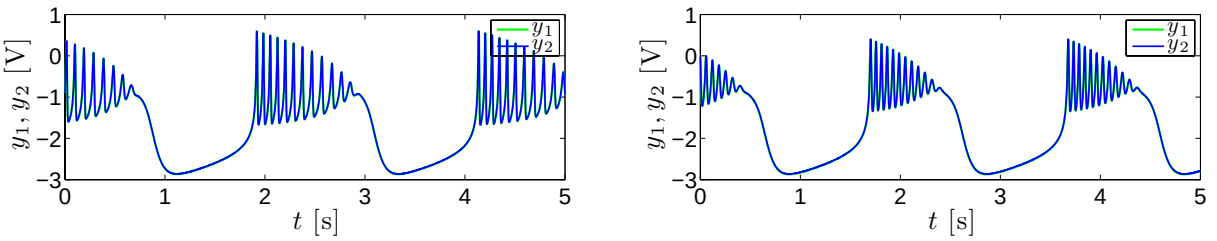

(a) $\sigma = 2\,[-]$, $\tau = 2\,[\text{ms}]$ (b) $\sigma = 4\,[-]$, $\tau = 2\,[\text{ms}]$

Fig. 6. Trajectories of two practically synchronized transmission delay coupled HR circuits for different values of σ and τ.

introduced because of the sampling of the coupling interface. All these imperfections are not taken into account in the theoretical framework. We emphasize once more that transmission delay coupling is *invasive*, contrary to the full delay coupling, which is *noninvasive*. Thus, the practically synchronized outputs of two full delay coupled electronic HR circuits look just like the ones depicted in Fig. 4(a). For transmission delay coupled circuits the shape of the synchronized outputs changes when the values of σ and τ are changed. This is depicted in Fig. 6, which shows experimental results of practically synchronized outputs of two transmission delay coupled HR circuits for $\sigma = 2\,[-]$ and $\tau = 2\,[\text{ms}]$, and $\sigma = 4\,[-]$ and $\tau = 2\,[\text{ms}]$.

5. Practical Synchronization and Practical Partial Synchronization in Networks of HR Circuits

In networks with more than two circuits, we may encounter, at least in theory, the partial synchronization phenomenon. Next, analogous to the definition of *practical synchronization*, we define *practical partial synchronization*:

Definition 5.1 [Practical Partial Synchronization]. Consider a network of k dynamical systems with outputs $y_i(t) \in \mathbb{R}^m$, $i \in \mathcal{V}$, defined on an interval $[t_0, t_2)$. The network of systems is said to *practically partially synchronize with bound* ϵ if there is a $t_1 = t_1(\epsilon)$, $t_0 \le t_1(\epsilon) < t_2$, such that $|y_i(t) - y_j(t)| < \epsilon$ holds for all $t \in [t_1, t_2)$ and at least two but not all $i, j \in \mathcal{V}$, $i \neq j$.

As before, we fix $\epsilon = 0.25\,[\text{V}]$ and refer to *practical partial synchronization with bound* ϵ as *practical partial synchronization*. We present three experimental studies on practical (partial) synchronization for:

(1) The network shown in Fig. 7 with four transmission delay coupled HR neurons.
(2) The network shown in Fig. 10 with four transmission delay coupled HR neurons.
(3) The network shown in Fig. 13 with ten full delay coupled HR neurons.

5.1. *Experiment 1*

Consider four transmission delay coupled HR circuits with the network topology depicted in Fig. 7. This network topology is taken from [Steur *et al.*, 2012], where it is shown, theoretically and using numerical simulations, that this network exhibits partial synchronization. It is easy to verify that each permutation matrix

$$\Pi_1 = \begin{pmatrix} \mathcal{J} & \mathbf{0} \\ \mathbf{0} & \mathcal{J} \end{pmatrix}, \quad \Pi_2 = \begin{pmatrix} \mathbf{0} & I_2 \\ I_2 & \mathbf{0} \end{pmatrix},$$

$$\Pi_3 = \begin{pmatrix} \mathbf{0} & \mathcal{J} \\ \mathcal{J} & \mathbf{0} \end{pmatrix},$$

with $\mathbf{0} = \mathbf{0}_{2\times 2}$ and

$$\mathcal{J} = \begin{pmatrix} 0 & 1 \\ 1 & 0 \end{pmatrix},$$

commutes with the weighted adjacency matrix

$$A = \frac{1}{3}\begin{pmatrix} 0 & 1 & 0 & 2 \\ 1 & 0 & 2 & 0 \\ 0 & 2 & 0 & 1 \\ 2 & 0 & 1 & 0 \end{pmatrix}.$$

By Lemma 1, $\mathcal{P}(\Pi_1)$, $\mathcal{P}(\Pi_2)$, and $\mathcal{P}(\Pi_3)$ are partial synchronization manifolds. The manifold $\mathcal{P}(\Pi_1)$ is associated with partial synchronization of neurons 1 and 2, respectively, neurons 3 and 4, manifold $\mathcal{P}(\Pi_2)$ corresponds to partial synchronization of neurons 1 and 3, respectively, neurons 2 and 4.

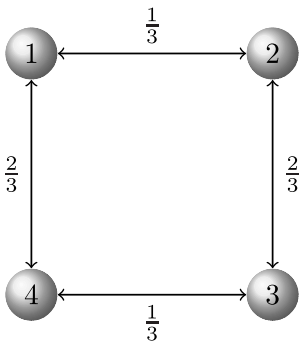

Fig. 7. The network topology for practical (partial) synchronization in Experiment 1.

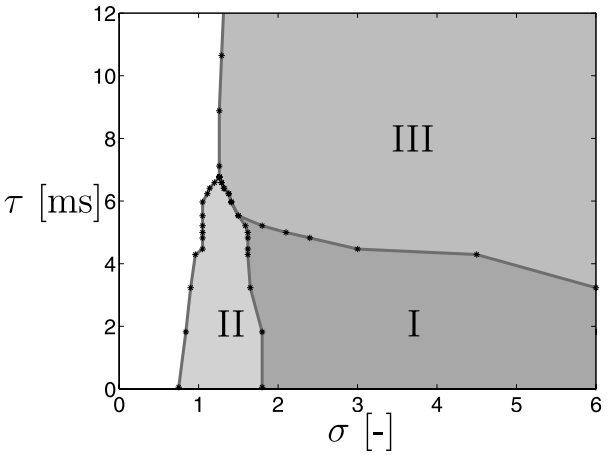

Fig. 8. Practical partial synchronization diagram for four transmission delay coupled HR circuits with network structure shown in Fig. 7. Crosses (∗) indicate measured boundary points of a practical (partial) synchronization regime. I. Practical synchronization, II. Practical partial synchronization of circuits 1 and 4, respectively, circuits 2 and 3, III. Practical partial synchronization of circuits 1 and 3, respectively, circuits 2 and 4.

Finally, manifold $\mathcal{P}(\Pi_3)$ defines partial synchronization of neurons 1 and 4, respectively, neurons 2 and 3. Then Theorem 3 implies, as $c^* \geq 1-\lambda_2(A) > 0$ by Proposition 1 in the Appendix, we may find partial synchronization in this network. It is shown in [Steur *et al.*, 2012, Sec. 7A], that the conditions for a (submanifold of) $\mathcal{P}(\Pi_1)$ to be stable coincide with the conditions for full synchronization. One can verify this using Proposition 1. It is also shown, using numerical simulations, that there exist values for the coupling strength σ and time-delay τ for which $\mathcal{P}(\Pi_2)$ and $\mathcal{P}(\Pi_3)$ are stable without having full synchronization. As it is shown below, our experiments confirm the theoretical and numerical findings presented in [Steur *et al.*, 2012]. We have explored the (σ, τ)-parameter space to identify the regions of practical synchronization and practical partial synchronization. Figure 8 depicts the results of these experiments. It is worth mentioning that our theoretical results imply the existence of a constant $\chi^* > 0$ such that circuits 1 and 3, respectively, circuits 2 and 4 partially synchronize for $\sigma\tau \leq \chi^*$ (provided $\sigma \geq \sigma^*$), but, as we did not encounter a loss of practical partial synchronization when τ was increased, our experiments seem to imply that this bound is not sharp. Figure 9 shows outputs of the practically partially synchronized HR circuits for different values of σ and τ. The top panel of Fig. 9(a) shows practically partially synchronized outputs of the HR circuits for $\sigma = 1.2\,[-]$, $\tau = 2\,[\text{ms}]$ (parameters in region II in Fig. 8). The four smaller plots provide an alternative graphical representation of practical partial synchronization. In these plots, we see that two circuits i and j are practically synchronized if their outputs $y_i(t)$ [V] and $y_j(t)$ [V] are within a 2ϵ-band centered around the diagonal in the (y_i, y_j)-plane. The diagonal and the bounds for practical synchronization are indicated by the dotted and dashed lines, respectively. These four plots show clearly the practical partial synchronization of circuits 1 and 4, respectively, circuits 2 and 3. Figure 9(b) shows the outputs of the four transmission delay coupled HR circuits for $\sigma = 4\,[-]$ and $\tau = 8\,[\text{ms}]$ (parameters in region III in Fig. 8), for which circuits 1 and 3, respectively, circuits 2 and 4 practically partially synchronize.

5.2. *Experiment 2*

Consider four HR circuits with full delay coupling on the network depicted in Fig. 10. The Laplacian matrix is given by

$$L = \frac{1}{3}\begin{pmatrix} 3 & -1 & -1 & -1 \\ -1 & 2 & -1 & 0 \\ -1 & -1 & 2 & 0 \\ -1 & 0 & 0 & 1 \end{pmatrix}.$$

The permutation matrix

$$\Pi = \begin{pmatrix} 1 & 0 & 0 & 0 \\ 0 & 0 & 1 & 0 \\ 0 & 1 & 0 & 0 \\ 0 & 0 & 0 & 1 \end{pmatrix}$$

commutes with L; hence, by Lemma 1, $\mathcal{P}(\Pi)$ is a partial synchronization manifold that corresponds

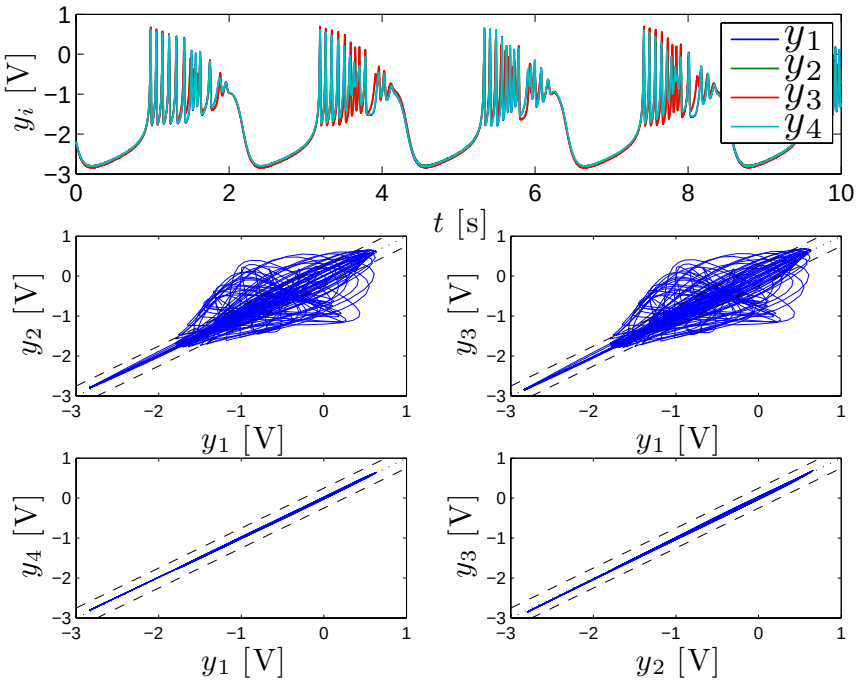

(a)

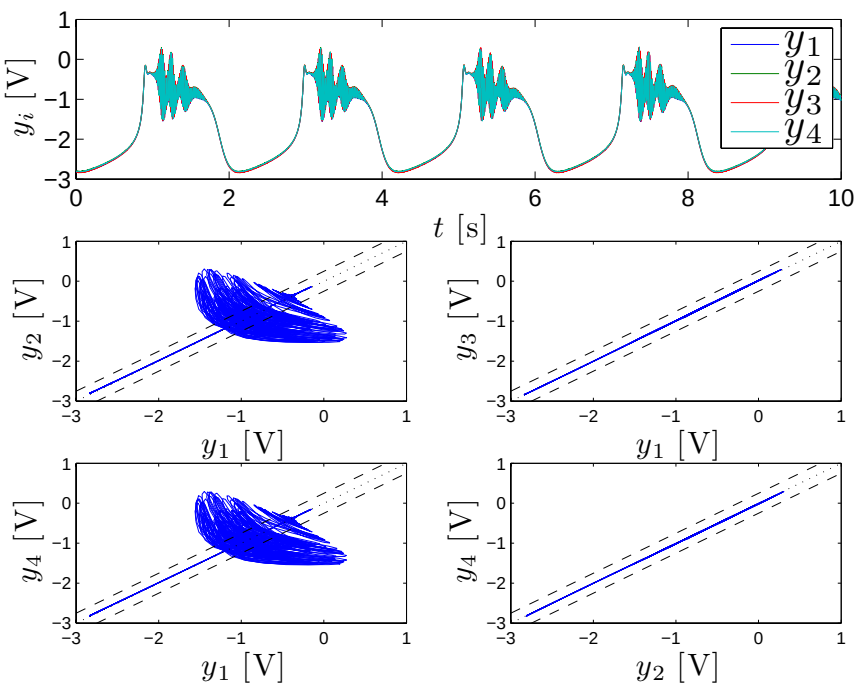

(b)

Fig. 9. Outputs of practical partially synchronized transmission delay coupled HR circuits. (a) Practical partial synchronization of circuits 1 and 4, respectively, 2 and 3 for $\sigma = 1.2\,[-]$ and $\tau = 2\,[\text{ms}]$ and (b) practical partial synchronization of circuits 1 and 3, respectively, 2 and 4 for $\sigma = 4\,[-]$ and $\tau = 8\,[\text{ms}]$.

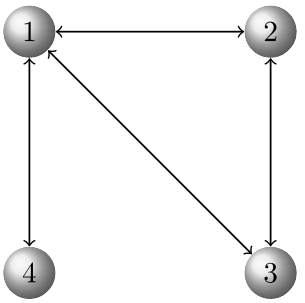

Fig. 10. The network topology for practical (partial) synchronization in Experiment 2. All edges have weight 1/3.

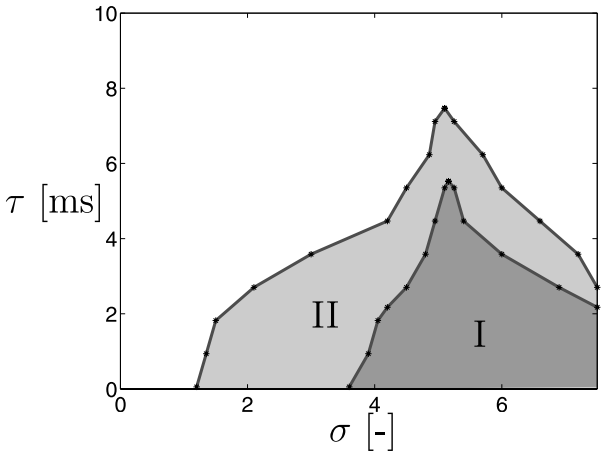

Fig. 11. Practical partial synchronization diagram for four full delay coupled HR circuits with network structure shown in Fig. 10. Crosses (∗) indicate measured boundary points of the practical (partial) synchronization regimes. (I) Practical full synchronization and (II) practical partial synchronization of circuits 2 and 3.

to partial synchronization of circuits 2 and 3. The numerical results presented in Sec. 6 of [Steur *et al.*, 2012] imply that this partial synchronization manifold is asymptotically stable for values of the coupling strength and time-delay that do not coincide with those for which we find full synchronization. One can indeed verify this using Proposition 2 in Appendix A. The experimentally determined practical (partial) synchronization diagram for the four full delay coupled HR circuits is shown in Fig. 11. Figure 12 shows output trajectories of the partially practically synchronized HR circuits for $\sigma = 3\,[-]$ and $\tau = 1.5\,[\text{ms}]$. Note that the parameter region that corresponds to practical full synchronization of the network is enclosed in the parameter region for partial practical synchronization of circuits 2 and 3, which confirms the theoretical prediction of Theorem 4 in combination with Proposition 2.

5.3. *Experiment 3*

Consider ten full delay coupled HR circuits on the network topology shown in Fig. 13. This network topology, which we refer to as the "sandglass network", was introduced in [Neefs *et al.*, 2010] in a study of partial synchronization of delay-free coupled HR neurons. However, a full analysis of the observed partial synchronization was not presented in that paper. We present the full analysis below. The Laplacian matrix of the sandglass network is

$$L = \frac{1}{2}\begin{pmatrix} 2 & -1 & 0 & -1 & 0 & 0 & 0 & 0 & 0 & 0 \\ -1 & 4 & -1 & -1 & -1 & 0 & 0 & 0 & 0 & 0 \\ 0 & -1 & 2 & 0 & -1 & 0 & 0 & 0 & 0 & 0 \\ 0 & -1 & 0 & 5 & -1 & -1 & -1 & 0 & 0 & 0 \\ 0 & -1 & -1 & -1 & 5 & -1 & -1 & 0 & 0 & 0 \\ 0 & 0 & 0 & -1 & -1 & 5 & -1 & -1 & -1 & 0 \\ 0 & 0 & 0 & -1 & -1 & -1 & 5 & 0 & -1 & -1 \\ 0 & 0 & 0 & 0 & 0 & -1 & 0 & 2 & -1 & 0 \\ 0 & 0 & 0 & 0 & 0 & -1 & -1 & -1 & 4 & -1 \\ 0 & 0 & 0 & 0 & 0 & 0 & -1 & 0 & -1 & 2 \end{pmatrix}.$$

We remark that $\max_i \sum_{j\in\mathcal{N}_i} a_{ij} = 5/2$, which violates our assumption $\max_i \sum_{j\in\mathcal{N}_i} a_{ij} = 1$. This violation is done for practical purposes; when $\max_i \sum_{j\in\mathcal{N}_i} a_{ij} = 1$, the coupling strength that is required for practical synchronization of all circuits would already be close to the maximal coupling strength in the experimental setup ($\sigma = 10\,[-]$). Moreover, from a theoretical point of view, the factor 5/2 could be absorbed in the coupling strength σ (by redefining σ); hence, violating the assumption

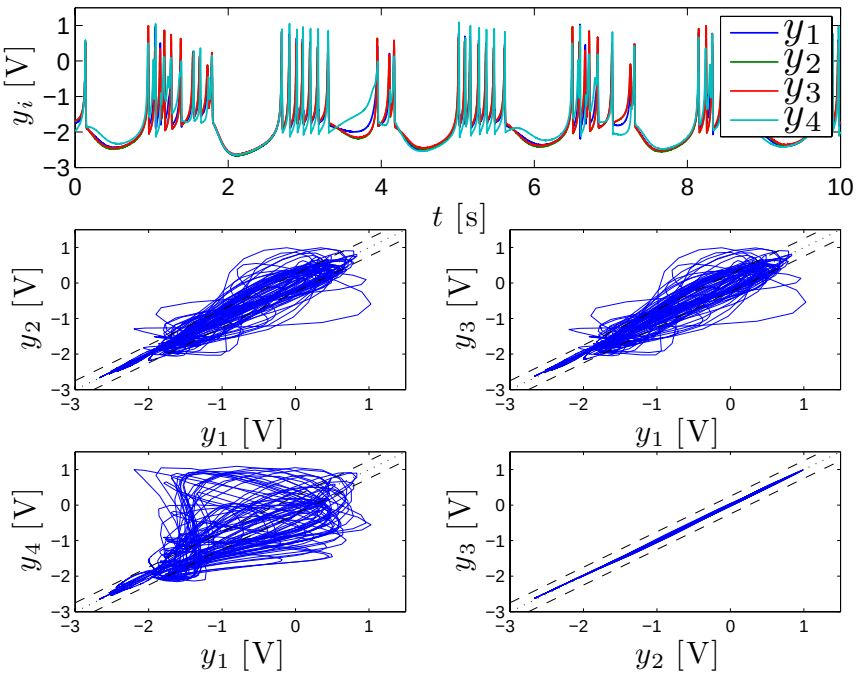

Fig. 12. Outputs of practical partially synchronized full delay coupled HR circuits 2 and 3 for $\sigma = 3\,[-]$ and $\tau = 1.5\,[\text{ms}]$ (region II in Fig. 11).

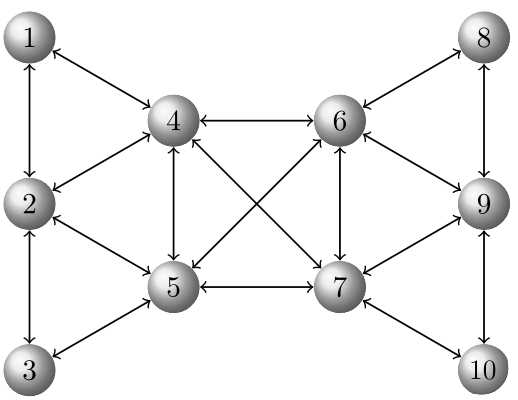

Fig. 13. The sandglass network topology for practical (partial) synchronization in Experiment 3. All edges have weight 1/2.

of $\max_i \sum_{j\in\mathcal{N}_i} a_{ij} = 1$ has no consequences for our theoretical results. (Of course, for the theoretical results we have to redefine $\sigma_{\max}$, $\overline{\sigma}$, $\overline{\chi}$, σ' and χ' accordingly).

The sandglass network contains a lot of partial synchronization manifolds. The permutation matrices that correspond to

- swapping of 1 and 8, 2 and 9, 3 and 10, 4 and 6, 5 and 7;
- swapping of 1 and 10, 2 and 9, 3 and 8, 4 and 7, 5 and 6;
- swapping 1 and 3 while keeping the others fixed;
- swapping 4 and 5 while keeping the others fixed;
- swapping 6 and 7 while keeping the others fixed;
- swapping 8 and 10 while keeping the others fixed;

and any combination of the latter four, e.g. simultaneous swapping of 1 and 3, and 4 and 5, define partial synchronization manifolds. This can all be easily verified using Lemma 1. Indeed, the Laplacian matrix of the sandglass network has eigenvalues

$$\lambda_1 = 0, \quad \lambda_2 = 0.39, \quad \lambda_3 = \lambda_4 = 0.88,$$

$$\lambda_5 = 1.5, \quad \lambda_6 = 2.22, \quad \lambda_7 = 2.5,$$

$$\lambda_8 = \lambda_9 = 3.11, \quad \lambda_{10} = 3.37,$$

with corresponding eigenvectors

$$\mu_1 = \mathbf{1}_{10\times 1},$$

$$\mu_2 = (a_2 \quad b_2 \quad a_2 \quad c_2 \quad c_2 \quad -c_2 \quad -c_2 \quad -a_2 \quad -b_2 \quad -a_2)^T,$$

$$\mu_3 = (a_3 \quad 0 \quad -a_3 \quad b_3 \quad -b_3 \quad c_3 \quad -c_3 \quad d_3 \quad 0 \quad -d_3)^T,$$

$$\mu_4 = (a_4 \quad 0 \quad -a_4 \quad b_4 \quad -b_4 \quad c_4 \quad -c_4 \quad d_4 \quad 0 \quad -d_4)^T,$$
$$\mu_5 = (a_5 \quad 0 \quad a_5 \quad -a_5 \quad -a_5 \quad -a_5 \quad -a_5 \quad a_5 \quad 0 \quad a_5)^T,$$
$$\mu_6 = (a_6 \quad b_6 \quad a_6 \quad c_6 \quad c_6 \quad -c_6 \quad -c_6 \quad -a_6 \quad -b_6 \quad -a_6)^T,$$
$$\mu_7 = (a_7 \quad b_7 \quad a_7 \quad a_7 \quad a_7 \quad a_7 \quad a_7 \quad a_7 \quad b_7 \quad a_7)^T,$$
$$\mu_8 = (a_8 \quad 0 \quad -a_8 \quad b_8 \quad -b_8 \quad c_8 \quad -c_8 \quad d_8 \quad 0 \quad -d_8)^T,$$
$$\mu_9 = (a_9 \quad 0 \quad -a_9 \quad b_9 \quad -b_9 \quad c_9 \quad -c_9 \quad d_9 \quad 0 \quad -d_9)^T,$$
$$\mu_{10} = (a_{10} \quad b_{10} \quad a_{10} \quad c_{10} \quad c_{10} \quad -c_{10} \quad -c_{10} \quad -a_{10} \quad -b_{10} \quad -a_{10})^T,$$

with $a_2, a_3, \ldots, b_2, b_3, \ldots, c_2, c_3, \ldots, d_2, \ldots, d_{10}$, being nonzero constants. The values of these constants are, of course, not arbitrary, but for our purpose there is no need to specify these; we only need to look at the repeating patterns in the eigenvectors. One observes that the linear span of eigenvectors μ_1, μ_2, μ_5, μ_6, μ_7 and μ_{10} is the set $\ker(I-\Pi)$ with permutation matrix

$$\Pi = \begin{pmatrix} 0 & 0 & 1 & 0 & 0 & 0 & 0 & 0 & 0 & 0 \\ 0 & 1 & 0 & 0 & 0 & 0 & 0 & 0 & 0 & 0 \\ 1 & 0 & 0 & 0 & 0 & 0 & 0 & 0 & 0 & 0 \\ 0 & 0 & 0 & 0 & 1 & 0 & 0 & 0 & 0 & 0 \\ 0 & 0 & 0 & 1 & 0 & 0 & 0 & 0 & 0 & 0 \\ 0 & 0 & 0 & 0 & 0 & 0 & 1 & 0 & 0 & 0 \\ 0 & 0 & 0 & 0 & 0 & 1 & 0 & 0 & 0 & 0 \\ 0 & 0 & 0 & 0 & 0 & 0 & 0 & 0 & 0 & 1 \\ 0 & 0 & 0 & 0 & 0 & 0 & 0 & 0 & 1 & 0 \\ 0 & 0 & 0 & 0 & 0 & 0 & 0 & 1 & 0 & 0 \end{pmatrix}.$$

Thus, $\ker(I-\Pi)$ is an invariant subspace of L such that, by Lemma 1, $\mathcal{P}(\Pi)$ is a partial synchronization manifold. Moreover, Π and L commute and the eigenvectors $\mu_3, \mu_4, \mu_8, \mu_9 \in \text{range}(I-\Pi)$ such that, by Proposition 2 in Appendix A, we may find partial synchronization of neurons 1 and 3, 4 and 5, 6 and 7, and 8 and 10. A repetition of this procedure shows that this is the only mode of partial synchronization that may be observed in this network. Figure 14 shows the experimentally determined practical (partial) synchronization diagram for the sandglass network. We see that circuits 1 and 3, respectively, 4 and 5, respectively, 6 and 7, respectively, 8 and 10 practically partially synchronize when the coupling is not strong enough to achieve practical full synchronization and in case the coupling is strong enough for practical full synchronization but the time-delay is too large. The shape of this practical partial synchronization diagram could have been expected because the smallest (largest) eigenvalue of L with eigenvector in $\text{range}(I-\Pi)$ is larger (smaller) than the smallest (largest) eigenvalue of L. Output trajectories of the ten full delay coupled HR circuits with $\sigma = 2\,[-]$ and $\tau = 1\,[\text{ms}]$ are depicted in Fig. 15. In particular, Fig. 15(a) shows clearly that circuits 1 and 3, respectively, 4 and 5, respectively, 6 and 7, respectively, 8 and 10 practically synchronize. Figure 15(b) confirms that only these circuits practically partially synchronize. Since the Laplacian matrix L of the sandglass network is symmetric, the practical full synchronization diagram of full delay coupled HR circuits could have been predicted

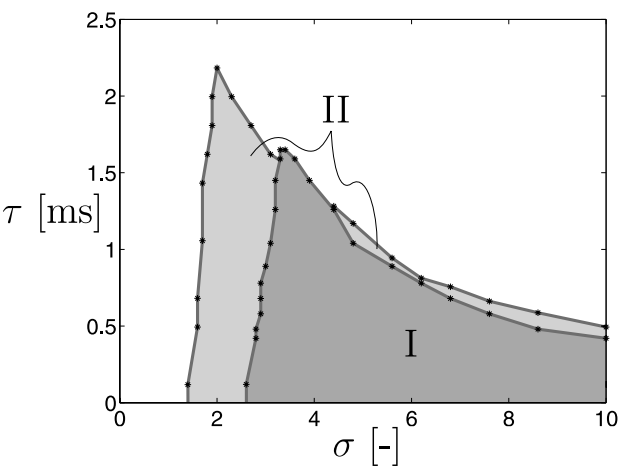

Fig. 14. Practical partial synchronization diagram for ten full delay coupled HR circuits on the sandglass network. Crosses (∗) indicate measured boundary points of the practical (partial) synchronization regimes. (I) Practical full synchronization; (II) practical partial synchronization of circuits 1 and 3, respectively, 4 and 5, respectively, 6 and 7, respectively, 8 and 10.

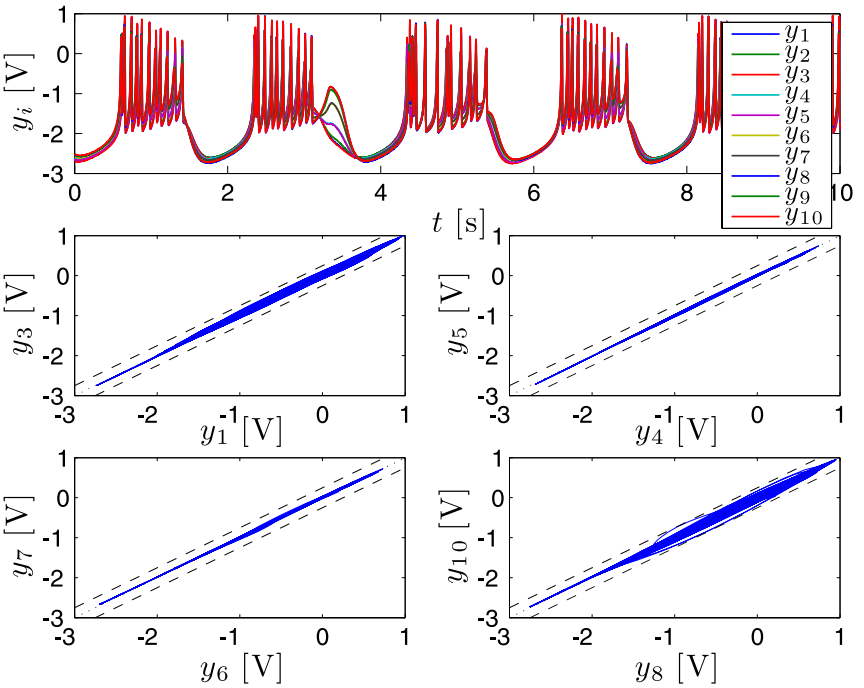

(a)

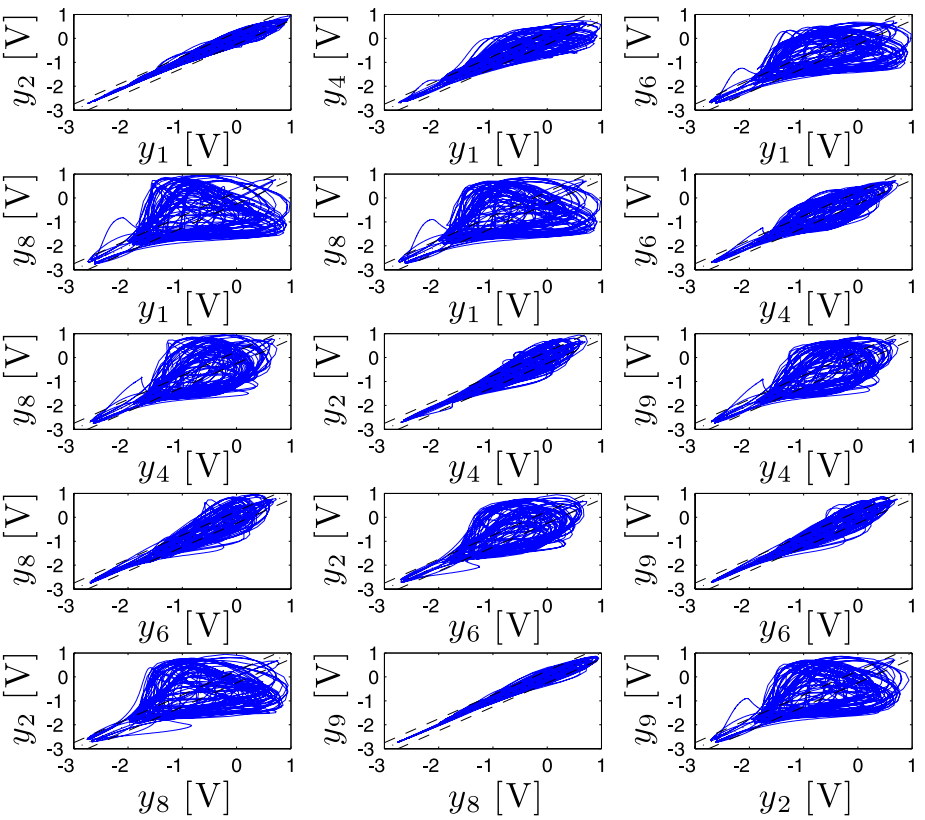

(b)

Fig. 15. Outputs of practical partially synchronized full delay coupled HR circuits for $\sigma = 2\,[-]$ and $\tau = 1\,[\mathrm{ms}]$ (region II in Fig. 14).

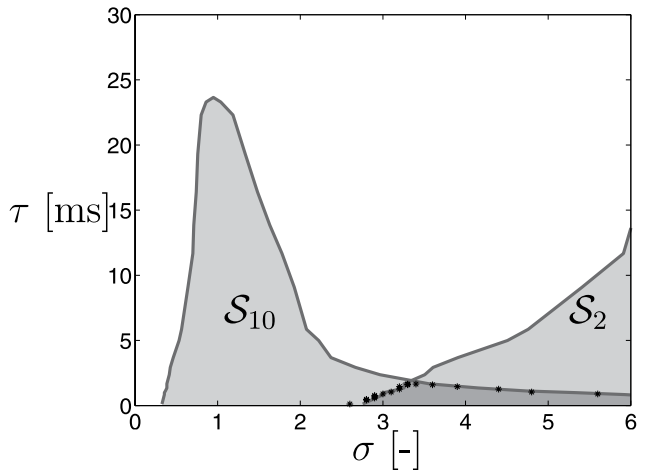

(a)

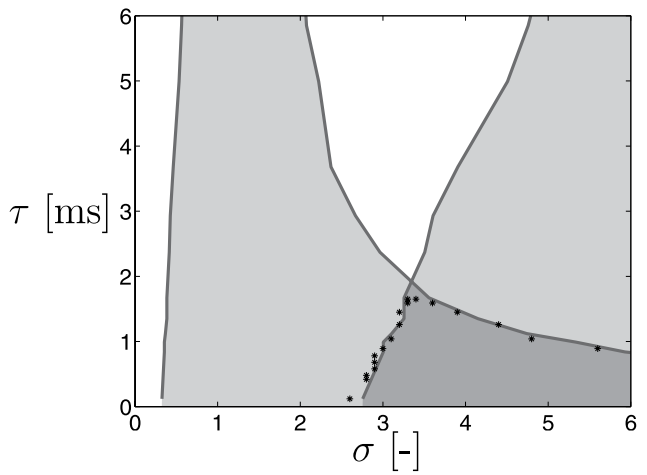

(b)

Fig. 16. Construction of the practical full synchronization diagram for the sandglass network with full delay coupling. (a) The scaled copies $\mathcal{S}_2$ and $\mathcal{S}_{10}$ of the practical synchronization diagram $\mathcal{S}^*$ shown in Fig. 5(b) (light shade), their intersection $\mathcal{S}_2 \cap \mathcal{S}_{10}$ (dark shade), and the (boundary of the) practical full synchronization diagram for the sandglass network ($*$). (b) Zoomed version of (a).

with the help of Theorem 2, from the practical synchronization diagram $\mathcal{S}^*$ shown in Fig. 5(b) for two coupled neurons. Indeed, as shown in Fig. 16, the intersection of two scaled copies $\mathcal{S}_2$ and $\mathcal{S}_{10}$ of that practical synchronization diagram, i.e. $\mathcal{S}_2$ is a copy of $\mathcal{S}^*$ scaled by a factor $2/\lambda_2 = 2/0.39$ over the σ-axis and $\mathcal{S}_{10}$ is another copy of $\mathcal{S}^*$ scaled by the factor $2/\lambda_{10} = 2/3.3733$ over the σ-axis, gives a reasonable accurate prediction of the practical full synchronization diagram for full delay coupled HR circuits on the sandglass network.

6. Concluding Remarks

We have studied synchronization and partial synchronization in networks of systems that interact via linear time-delay coupling. The predictive value of the theoretical results of [Steur & Nijmeijer, 2010; Steur *et al.*, 2012; Steur *et al.*, 2014a] is tested using an experimental setup built around electronic circuit board realizations of networks of HR neurons. To account for the inevitable dissimilarities in the electronic HR circuits, we have introduced the notions of *practical synchronization* and *practical partial synchronization*, which state that the circuits may be called (partially) synchronized if, after some transient time, the differences between their outputs are sufficiently small on a long finite time interval. In a first set of experiments, we have determined the practical synchronization diagrams for two HR circuits with transmission delay coupling and full delay coupling. In a next set of experiments, we investigated full practical synchronization and partial practical synchronization in networks of HR circuits with transmission delay coupling or full delay coupling. The first two experiments, in this set, used the settings of the numerical studies presented in [Steur *et al.*, 2012]. The sandglass network topology of the third experiment was introduced in [Neefs *et al.*, 2010]. Lastly, we successfully applied the theory presented in [Steur *et al.*, 2014a] to construct the full practical synchronization diagram in the sandglass network of full delay coupled HR circuits from the practical synchronization diagram of two full delay coupled HR circuits. These experimental results indicate that the theoretical results presented in [Steur & Nijmeijer, 2010; Steur *et al.*, 2012; Steur *et al.*, 2014a], which are derived for networks of noise-free identical systems, can be successfully applied to real-world applications. However, we have found that our theoretical results are not always sharp (see Experiment 1 in Sec. 5). We conclude that our theoretical results can predict network synchronization reasonably well in a *qualitative* sense, but its predictive power at a *quantitative* level can be rather poor. Practical applications often require constructive methods that allow for precise computations of the network parameters (coupling strength σ and time-delay τ) for given dynamical systems. The estimates that are computed from the proofs of the results of [Steur & Nijmeijer, 2010; Steur *et al.*, 2012; Steur *et al.*, 2014a] are however often too

conservative. Moreover, although the theory (which is developed under the assumption of identical systems and deterministic dynamics) predicts the experimental observations in most cases quite well, a theory that would give us formal predictions for (practical) synchronization in networks of systems that have mismatches and operate under noisy conditions is yet to be developed.

References

Agrawal, D., Thiruvenkatanathan, P., Yan, J. & Seshia, A. [2011] "Electrically coupled mems oscillators," *2011 Joint Conf. IEEE Int. Frequency Control and the European Frequency and Time Forum* (*FCS*), pp. 1–5.

Aihara, I., Takeda, R., Mizumoto, T., Otsuka, T., Takahashi, T. & Okuno, H. [2011] "Complex and transitive synchronization in a frustrated system of calling frogs," *Phys. Rev. E* **83**, 031913.

Belykh, V. N., Belykh, I. V. & Hasler, M. [2004] "Connection graph stability method for synchronized coupled chaotic systems," *Physica D* **195**, 159–187.

Belykh, I., Hasler, M., Lauret, M. & Nijmeijer, H. [2005] "Synchronization and graph topology," *Int. J. Bifurcation and Chaos* **15**, 3423–3433.

Blekhman, I. [1988] *Synchronization in Science and Technology* (ASME, NY).

Bollobas, B. [1998] *Modern Graph Theory* (Springer-Verlag, NY).

Czeisler, C. A., Weitzman, E. D., Moore-Ede, M. C., Zimmerman, J. C. & Knauer, R. S. [1980] "Human sleep: Its duration and organization depend on its circadian phase," *Science* **210**, 1264–1267.

Dahms, T., Lehnert, J. & Schöll, E. [2012] "Cluster and group synchronization in delay-coupled networks," *Phys. Rev. E* **86**, 016202.

Dorfler, F. & Bullo, F. [2012] "Synchronization and transient stability in power networks and non-uniform Kuramoto oscillators," *SIAM J. Contr. Optim.* **50**, 1616–1642.

Gray, C. [1994] "Synchronous oscillations in neuronal systems: Mechanisms and functions," *J. Comput. Neurosci.* **1**, 11–38.

Grzybowski, J., Macau, E. & Yoneyama, T. [2011] "Isochronal synchronization of time delay and delay-coupled chaotic systems," *J. Phys. A*: *Math. Theoret.* **44**, 175103.

Hale, J. [1997] "Diffusive coupling, dissipation, and synchronization," *J. Dyn. Diff. Eqs.* **9**, 17–31.

Hindmarsh, J. & Rose, R. [1984] "A model for neuronal bursting using three coupled differential equations," *Proc. Roy. Soc. Lond. B* **221**, 87–102.

Hoppensteadt, F. & Izhikevich, E. [2001] "Synchronization of mems resonators and mechanical neurocomputing," *IEEE Trans. Circuits Syst.-I* **48**, 133–138.

Hutu, F., Cauet, S. & Coirault, P. [2009] "Robust synchronization of different coupled oscillators: Application to antenna arrays," *J. Franklin Instit.* **346**, 413–430.

Koch, C. [1999] *Biophysics of Computation*, 1st edition (Oxford University Press).

Michiels, W. & Nijmeijer, H. [2009] "Synchronization of delay-coupled nonlinear oscillators: An approach based on the stability analysis of synchronized equilibria," *Chaos* **19**, 033110.

Murguia, C., Fey, R. & Nijmeijer, H. [2014] "Synchronization of identical linear systems and diffusive time-delayed couplings," *IEEE Trans. Circuits Syst.-I* **61**, 1801–1814.

Neefs, P., Steur, E. & Nijmeijer, H. [2010] "Network complexity and synchronous behavior — An experimental approach," *Int. J. Neural Syst.* **20**, 233–247.

Oguchi, T. & Nijmeijer, H. [2011] "A synchronization condition for coupled nonlinear systems with time-delay: A frequency domain approach," *Int. J. Bifurcation and Chaos* **21**, 2525–2538.

Olfati-Saber, R. & Murray, M. [2004] "Consensus problems in networks of agents with switching topology and time-delays," *IEEE Trans. Automat. Contr.* **49**, 1520–1533.

Pavlov, A., Pogromsky, A., van de Wouw, N. & Nijmeijer, H. [2004] "Convergent dynamics, a tribute to Boris Pavlovich Demidovich," *Syst. Contr. Lett.* **52**, 257.

Pecora, L. & Carroll, T. [1998] "Master stability functions for synchronized coupled systems," *Phys. Rev. Lett.* **80**, 2109–2112.

Peskin, C. [1975] *Mathematical Aspects of Heart Physiology* (Courant Institute of Mathematical Sciences, New York University), pp. 268–278.

Pikovsky, A., Rosenblum, M. & Kurths, J. [2001] *Synchronization*: *A Universal Concept in Nonlinear Science* (Cambridge University Press, Cambridge).

Ploeg, J., van de Wouw, N. & Nijmeijer, H. [2014] "Lp string stability of cascaded systems: Application to vehicle platooning," *IEEE Trans. Contr. Syst. Technol.* **22**, 786–793.

Pogromsky, A. [1998] "Passivity based design of synchronizing systems," *Int. J. Bifurcation and Chaos* **8**, 295–319.

Pogromsky, A. Y. [2008] "A partial synchronization theorem," *Chaos* **18**; Erratum: [2009] *Chaos* **19**, 049901.

Ren, W. & Atkins, E. [2007] "Distributed multi-vehicle coordinated control via local information exchange," *Int. J. Rob. Nonlin. Contr.* **17**, 1002–1033.

Rodriguez, A. & Nijmeijer, H. [2001] "Coordination of two robot manipulators based on position measurements only," *Int. J. Contr.* **74**, 1311–1323.

Sadowska, A., van den Broek, T., Huijberts, H., van de Wouw, N., Kostic'c, D. & Nijmeijer, H. [2011] "A virtual structure approach to formation control of unicycle mobile robots using mutual coupling," *Int. J. Contr.* **84**, 1886–1902.

Sheikholeslam, S. & Desoer, A. [1993] "Longitudinal control of a platoon of vehicles with no communication of lead vehicle information: A system level study," *IEEE Trans. Veh. Technol.* **42**, 546–554.

Sipahi, R., Niculescu, S., Abdallah, C. T., Michiels, W. & Gu, K. [2011] "Stability and stabilization of systems with time delay," *IEEE Contr. Syst.* **31**, 38–65.

Stankovic, S., Stanojevic, M. & Siljak, D. [2000] "Decentralized overlapping control of a platoon of vehicles," *IEEE Trans. Contr. Syst. Technol.* **8**, 816–832.

Steur, E., Tyukin, I. & Nijmeijer, H. [2009] "Semi-passivity and synchronization of diffusively coupled neuronal oscillators," *Physica D* **238**, 2119–2128.

Steur, E. & Nijmeijer, H. [2010] "Synchronization in networks of diffusively time-delay coupled (semi-)passive systems," *IEEE Trans. Circuits Syst.-I* **58**, 1358–1371.

Steur, E., Oguchi, T., van Leeuwen, C. & Nijmeijer, H. [2012] "Partial synchronization in diffusively time-delay coupled oscillator networks," *Chaos* **22**, 043144.

Steur, E., Michiels, W., Huijberts, H. & Nijmeijer, H. [2014a] "Networks of diffusively time-delay coupled systems: Conditions for synchronization and its relation to the network topology," *Physica D* **277**, 22–39.

Steur, E., van Leeuwen, C. & Michiels, W. [2014b] "Partial synchronization manifolds for linearly time-delayed coupled systems," *21st Int. Symp. Mathematical Theory of Networks and Systems* (*MTNS 2014*), Groningen, the Netherlands.

Strogatz, S. [2003] *SYNC. The Emerging Science of Spontaneous Order* (Hyperion, NY).

Ünal, H. & Michiels, W. [2013] "Prediction of partial synchronization in delay-coupled nonlinear oscillators, with application to Hindmarsh–Rose neurons," *Nonlinearity* **26**, 3101–3126.

Wang, Q., Duan, Z., Perc, M. & Chen, G. [2008] "Synchronization transitions on small-world neuronal networks: Effects of information transmission delay and rewiring probability," *EPL* (*Europhys. Lett.*) **83**, 50008.

Wang, Q., Perc, M., Duan, Z. & Chen, G. [2009] "Synchronization transitions on scale-free neuronal networks due to finite information transmission delays," *Phys. Rev. E* **80**, 026206.

Wang, Q., Chen, G. & Perc, M. [2011a] "Synchronous bursts on scale-free neuronal networks with attractive and repulsive coupling," *PLoS One* **6**, 15851.

Wang, Q., Murks, A., Perc, M. & Lu, Q. [2011b] "Taming desynchronized bursting with delays in the macaque cortical network," *Chinese Phys. B* **20**, 040504.

Winfree, A. [2001] *The Geometry of Biological Time*, 2nd edition, Interdisciplinary Applied Mathematics (Springer).

Wu, C. & Chua, L. [1995] "Synchronization in an array of linearly coupled dynamical systems," *IEEE Trans. Circuits Syst.-I* **42**, 430–447.

Wu, C. & Chua, L. [1996] "On a conjecture regarding the synchronization in an array of linearly coupled dynamical systems," *IEEE Trans. Circuits Syst.-I* **43**, 161–165.

Appendix A

Necessary Conditions for Partial Synchronization

Proposition 1 [Steur *et al.*, 2012]. *Assume that* $A = A^T$ *is the adjacency matrix of a simple and strongly connected graph, and that the row sums of* A *all equal* 1. *Then* A *has eigenvalues* $1 = \lambda_1 > \lambda_2 \geq \cdots \geq \lambda_k \geq -1$. *Given a permutation matrix* Π *that commutes with* A, *let* Λ_Π *be the set of eigenvalues of* A *with eigenvectors in the set* $\mathrm{range}(I - \Pi)$. *Then*

- $\sigma^* < \overline{\sigma}$ *only if the largest element of* Λ_Π *is strictly smaller than* λ_2;
- $\chi^* > \overline{\chi}$ *only if all elements of* Λ_Π *in absolute value are strictly smaller than* $\max\{|\lambda_2|, |\lambda_k|\}$.

Proposition 2 [Steur *et al.*, 2012]. *Suppose that* $L = L^T$ *is the Laplacian matrix of a simple and strongly connected graph. Then* L *has eigenvalues* $0 = \lambda_1 < \lambda_2 \leq \cdots \leq \lambda_k$. *Given a permutation matrix* Π *that commutes with* L, *let* Λ_Π *be the set of eigenvalues of* L *with eigenvectors in the set* $\mathrm{range}(I - \Pi)$. *Then*

- $\sigma^* < \overline{\sigma}$ *only if the smallest element of* Λ_Π *is strictly larger than* λ_2;
- $\chi^* > \overline{\chi}$ *only if all elements of* Λ_Π *are strictly smaller than* λ_k.